INTERNATIONAL JOURNAL OF PRECISION ENGINEERING AND MANUFACTURING Vol. 15, No. 12, pp. 2483-2491 DECEMBER 2014 / 2483
DOI: 10.1007/s12541-014-0618-0

Pose Measuring and Aligning of a Micro Glass Tube and a Hole on the Micro Sphere

Fu-Dong Li[1], De Xu[1,#], Zheng-Tao Zhang[1], Ya-Li Shi[1], and Fei Shen[1,2]

1 Research Center of Precision Sensing and Control, Institute of Automation, Chinese Academy of Sciences, Beijing, China, 100190
2 Laser Fusion Research Center, Chinese Academy of Engineering Physics, Mianyang, China, 621900
Corresponding Author / E-mail: sdxude@yahoo.com, TEL: +86-10-82544707, FAX: +86-10-82544535-806

KEYWORDS: Pose measuring, Pose aligning, Pose vector, Microscopic camera, Microassembly

To ensure high uniformity of the inner space of the hollow sphere after assembly, the glass tube must be inserted into the hole on the sphere towards the center of the sphere. This paper deals with the pose measuring of the hole on the sphere and the glass tube and pose aligning of the two objects. The sphere is 500 mm in diameter with a 20 mm hole on it, and the glass tube is 17 mm in diameter. Novel pose measuring method for the hole on the sphere and the glass tube is developed, using two microscopic cameras, each one acquires a projection vector of the object to be measured. A plane containing the optical axis of the microscopic camera and the pose vector of the object is determined, with the microscopic camera calibrated in advance. Pose vector of the object to be measured can be calculated by the intersection of the two planes acquired by the two microscopic cameras. Error analysis of the pose measuring method is conducted and experimental results were consistent with analytical results. Less than 0.7º pose aligning error is achieved using the proposed pose measuring method and pose aligning method.

Manuscript received: March 20, 2014 / Revised: July 6, 2014 / Accepted: July 27, 2014

NOMENCLATURE

$^{M}R_{cL}$ = rotary matrix between microscopic camera L coordinates and manipulator coordinates

$^{M}R_{cR}$ = rotary matrix between microscopic camera R coordinates and manipulator coordinates

k_{xL}, k_{yL}, k_{xR}, k_{yR} = pixel scale factors of microscopic camera L and microscopic camera R

θ_x = adjusting angle around x axis

θ_y = adjusting angle around y axis

AO_1 = pose vector of the hole on the sphere

BA_1 = pose vector of the glass tube

V_{zL} = optical axis of microscopic camera L

n_{HL} = normal vector of the plane containing pose vector of the hole on the sphere and optical axis of microscopic camera L

n_{TL} = normal vector of the plane containing pose vector of the glass tube and optical axis of microscopic camera L

V_{zR}, n_{HR}, n_{TR} = same meaning with V_{zL}, n_{HL}, n_{TL}, but of microscopic camera R

1. Introduction

The increasing functionalities and complexities of Micro-electro-mechanical Systems (MEMS) require the integration of components fabricated with different technologies, and microassembly technology is indispensible to fulfill the integration. Although microassembly technologies are gaining more and more attention, much attention is attached to the precise positioning of the micro components. The researches of pose measurement in microassembly are relatively developing slowly. While complex 3-D microassembly tasks requiring precise positioning of the micro components have been developed and improved,[1-6] pose measurement of micro components are mainly constrained to planar pose measurement, or rough estimation, or even, the pose of the micro component are manipulated in an open-loop manner.

There are some researches on pose measurement in the macro world. Position information and pose information of the capsule endoscope were measured by using 3 Hall-effect sensors orthogonally installed inside the capsule, and an additional Hall-effect sensor was employed to enhance the measurement accuracy.[7] But to install sensors in the micro component is not applicable. 3D model of the target was

used for projection to generate corresponding 2D template, then images acquired from the CCD were used to match with the dynamic-template-library to determine the target's pose.[8] A non-cooperative geostationary orbit (GEO) spacecraft pose measuring method based on binocular stereo vision was developed, which took the natural circular feature on the GEO satellite as the recognized object, and achieved less than 6.5× estimated errors in the simulation.[9] A new Kalman-based multicamera sensor fusion approach for pose estimation was developed that could offer higher accuracy and precision, and was robust to camera motion and image occlusion.[10] Colored markers arranged in a known geometry were used for pose estimation of a volant robot, which was low-cost and computationally inexpensive.[11] Artificial marks were designed for 3D pose measurement using monocular vision.[12] The above vision-based pose measuring researches are in the macro domain, and there is a big difference between the vision systems for macro manipulation and micro manipulation. Depth of field of the microscopic camera used in microassembly is very small, and only part of the object to be measured can have a clear view. This drawback makes pose measurement in microassembly a difficult task.

High precision for pose measuring can be realized by using laser interferometer. 10 mrad pitch errors was achieved for a computer numerical control measurement using a laser interferometer.[13] But the angular module should be attached to the object to be measured, and it is impossible to attach such a big module to a micro sized component. Scanning electron microscope, scanning tunneling microscope and atomic force microscope can detect up to nano meter position precision of a micro component, and with the help of a precise motion platform, the pose of a micro component can be measure with high accuracy. But these equipments are difficult to be integrated into a microassembly system.

From the existed literature, pose measuring techniques in microassembly have been developing relatively slowly. A method for measuring the position and pose of the hohlraum fusing 3 CCDs information was raised,[14] and less than 1 mm accuracy was achieved. But for the pose measurement of the hohlraum, only a theoretical method with many constraints was proposed, and no relative experimental results were mentioned. In a 3D rotary optical switch assembly task,[15] the pose of the micro mirror was measured and adjusted using a pushing-based operation. But the pose estimation and adjust was one dimensional, around y axis of the predefined coordinates, 3D pose information of the micro mirror was not measured.

In our microassembly task, which is to insert a 17 mm diameter glass tube into a 20 mm diameter hole on a 500 mm diameter sphere, the glass tube is required to be inserted into the sphere in a pose towards the center of the sphere, to ensure the high quality of the microassembly. To realize the requirement of the microassembly task, we develop a novel method to measure the pose of the hole on the sphere and the pose of the glass tube.

The rest of the paper is organized as follows. Section 2 gives a brief introduction of the system setup. In section 3, the pose measuring method for the hole on the sphere and the glass tube is elaborated. Section 4 gives error analysis for pose measuring of the proposed method. Pose aligning method is described in Section 5, and experimental results are presented in section 6. Finally, the paper is concluded in section 7.

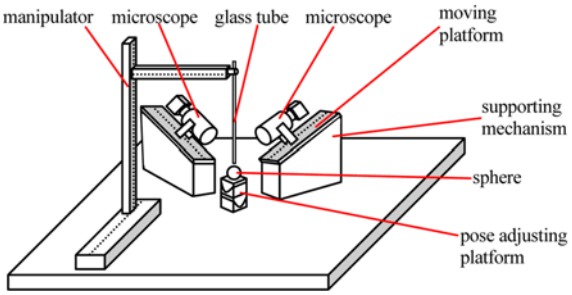

Fig. 1 Illustration of the system setup

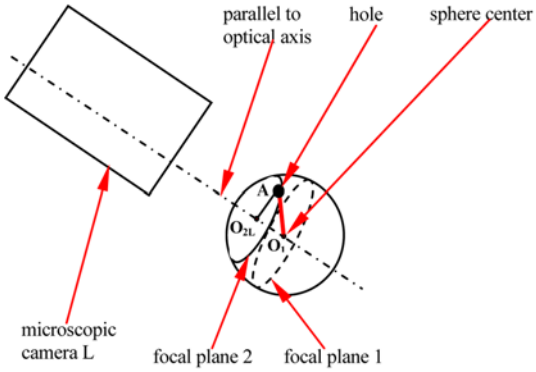

Fig. 2 Illustration of the pose measuring for the hole on the sphere

2. System Setup

The pose aligning system consists of a vision unit, a pose adjusting unit, and a host computer to analyze the image information and control the pose adjusting process.

The vision unit consists of two microscopic cameras each with a moving platform along its optical axis. The pose adjusting unit has two degrees of freedom, rotation around x axis of the 3-DOF manipulator coordinates, and rotation around y axis of the manipulator coordinates.

3. Hole and Tube Pose Measuring Method

3.1 Pose measuring method for the hole on the sphere

The pose measuring for the hole on the sphere is illustrated in Fig. 2. Focal plane 1 is the plane containing an equator of the sphere and it is perpendicular to the optical axis of microscopic camera L. The center of the sphere is on focal plane 1. Focal plane 2 is parallel to focal plane 1 and it contains the center of the hole. O_1 is the center of the sphere, and O_{2L} is the projection of O_1 on focal plane 2. Point A is the center of the hole.

The pose measuring for the hole on the sphere has 3 steps:

Step 1: Microscopic camera L is moved along its optical axis, and the equator of the sphere vertical to the optical axis of microscopic camera L is focused. Edge points on the equator of the sphere are selected, and least-square circle fitting of the selected edge points are conduct to determine the center of the sphere O_1.

Step 2: Microscopic camera L is moved along its optical axis, and

center of the hole is focused. The center of the sphere O_1 has a projection point O_{2L} on focal plane 2, where the clear part is the hole center. Since the motion from focal plane 1 to focal plane 2 is along the optical axis of microscopic camera L and the length of the motion is small, the coordinates of O_{2L} is considered to be the same as O_1 on the image.

Step 3: Calculation of the pose vector of the hole on the sphere.

Vector $AO_{2L} = [Dx_{mL}, Dy_{mL}, Dz_{mL}]^T$ in the manipulator coordinates can be calculated, from the image captured by microscopic camera L,

$$\begin{cases} \Delta x_{mL} = n_{xL}k_{xL}\Delta u_L + o_{xL}k_{yL}\Delta v_L \\ \Delta y_{mL} = n_{yL}k_{xL}\Delta u_L + o_{yL}k_{yL}\Delta v_L \\ \Delta z_{mL} = n_{zL}k_{xL}\Delta u_L + o_{zL}k_{yL}\Delta v_L \end{cases} \quad (1)$$

where, n_{xL}, n_{yL}, n_{zL}, o_{xL}, o_{yL}, o_{zL} are the elements in the rotary matrix between microscopic camera L coordinate and the manipulator coordinate, k_{xL}, k_{yL} are pixel scale factors of microscopic camera L, Du_L, Dv_L are the deviations between A and O_{2L} on the image. The rotary matrix and the pixel scale factors are calibrated in the following way. The tip of the glass tube is controlled to move on the focal plane of the microscopic camera for two steps using autofocus technique. By transforming the two vectors formed by the two steps on the image into two vectors along axes and conducting same transformation to the two vectors formed by the two steps in the manipulator coordinates, the pixel scale factors and rotary matrix can be calculated. For more details, see Ref. 16.

With the vector AO_{2L} calculated and the vector along optical axis of microscopic camera L calibrated in advance, the normal vector to plane O_1AO_{2L} can be calculated

$$n_{HL} = AO_{2L} \times V_{zL} \quad (2)$$

where, $V_{zL} = [a_{xL}, a_{yL}, a_{zL}]^T$ is the optical axis of microscopic camera L expressed in the manipulator coordinates, n_{HL} is the normal vector of the plane O_1AO_{2L}.

The vector n_{HL} is obtained from the image information of microscopic camera L. In the same way, we can obtain a similar vector n_{HR} from the image information of microscopic camera R. Both the vector n_{HL} and n_{HR} is vertical to vector AO_1, so the pose of the hole can be calculated.

$$AO_1 = n_{HL} \times n_{HR} \quad (3)$$

3.2 Pose measuring method for the glass tube

Pose measuring for the glass tube is similar to pose measuring for the hole on the sphere, and it is illustrated in Fig. 3.

The pose measuring for the glass tube also has 3 steps:

Step 1: Microscopic camera L is moved along its optical axis, and a suitable part of the glass tube is focused. Center point of the glass tube's clear part on the image is selected on the image as A_1.

Step 2: Microscopic camera L is moved along its optical axis, and another part of the glass tube is focused. The first selected point A_1 has a projection point A_{2L} on focal plane 2. At this time, the clear center point of the glass tube is B.

Step 3: Calculation of the pose vector of the glass tube.

Vector BA_{2L} in the manipulator coordinates can be calculate0.4 from the image captured by microscopic camera L, according to (1).

Then the normal vector to the plane A_1BA_{2L} can be calculated

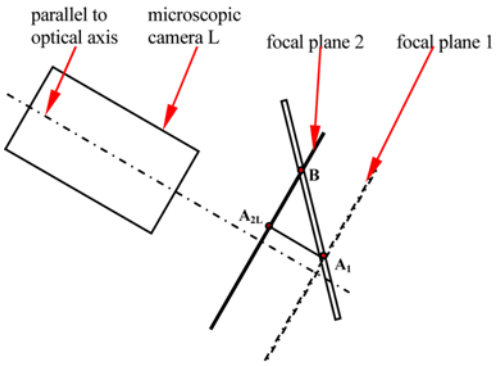

Fig. 3 Illustration of the pose measuring for the glass tube

$$n_{TL} = BA_{2L} \times V_{zL} \quad (4)$$

Vector n_{TL} is obtained from the image information of microscopic camera L. Similarly, we can obtain a vector n_{TR} from the image information of microscopic camera R. Both the vector n_{TL} and n_{TR} is vertical to the vector BA_1, so the pose of the glass tube can be calculated.

$$BA_1 = n_{TL} \times n_{TR} \quad (5)$$

4. Error Analysis

During the pose measuring process, feature points on the image are selected manually. Suppose the error of the selected point on the image from the ideal point is (du_L, dv_L) for microscopic camera L, and (du_R, dv_R) for microscopic camera R.

Vector $AO'_{2L} = [\Delta x'_{mL}, \Delta y'_{mL}, \Delta z'_{mL}]^T$ is

$$\begin{cases} \Delta x'_{mL} = n_{xL}k_{xL}(\Delta u_L + du_L) + o_{xL}k_{yL}(\Delta v_L + dv_L) \\ \Delta y'_{mL} = n_{yL}k_{xL}(\Delta u_L + du_L) + o_{yL}k_{yL}(\Delta v_L + dv_L) \\ \Delta z'_{mL} = n_{zL}k_{xL}(\Delta u_L + du_L) + o_{zL}k_{yL}(\Delta v_L + dv_L) \end{cases} \quad (6)$$

Normal vector n'_{HL} is calculated to be:

$$\begin{aligned} n'_{HL} &= AO'_{2L} \times V'_{zL} \\ &= [\Delta x'_{mL}, \Delta y'_{mL}, \Delta z'_{mL}]^T \times [a_{xL}, a_{yL}, a_{zL}]^T \\ &= [\Delta n'_{mLx}, \Delta n'_{mLy}, \Delta n'_{mLz}]^T \end{aligned} \quad (7)$$

Normal vector n'_{HR} is calculated with the information of microscopic camera R.

$$\begin{aligned} n'_{HR} &= AO'_{2R} \times V'_{zR} \\ &= [\Delta x'_{mR}, \Delta y'_{mR}, \Delta z'_{mR}]^T \times [a_{xR}, a_{yR}, a_{zR}]^T \\ &= [\Delta n'_{mRx}, \Delta n'_{mRy}, \Delta n'_{mRz}]^T \end{aligned} \quad (8)$$

Pose vector of the hole AO'_1 is:

$$\begin{aligned} AO'_1 &= n'_{HL} \times n'_{HR} \\ &= [\Delta n'_{mLx}, \Delta n'_{mLy}, \Delta n'_{mLz}]^T \times [\Delta n'_{mRx}, \Delta n'_{mRy}, \Delta n'_{mRz}]^T \\ &= [ao_{1x}, ao_{1y}, ao_{1z}]^T \end{aligned} \quad (9)$$

Detailed expression of Eq. (7)~(9) are shown in appendix.

When the coordinates of point A and O_{2L} in microscopic camera L and point A and O_{2R} in microscopic camera R are determined, (Du_L, Dv_L) and (Du_R, Dv_R) can be calculated. Pose vector of the hole with errors, AO'_1, can be calculated by substituting (Du_L, Dv_L), (Du_R, Dv_R), (du_L, dv_L) and (du_R, dv_R) into Eq. (9). Pose error caused by image errors can be determined by comparison of AO'_1 and AO_1,.

Pose error analysis for the glass tube is similar to pose error analysis for the hole. Pose vector of the glass tube with errors, BA'_1, shares the same expression with AO'_1.

The maximum error is investigated as follows. For example, microscopic camera L and R are calibrated. Rotary matrix from microscopic camera L and R coordinates to manipulator coordinates are

$$ {}^{M}R_{CL} = \begin{bmatrix} -0.999 & 0.012 & -0.054 \\ -0.051 & -0.514 & 0.856 \\ -0.019 & 0.858 & 0.514 \end{bmatrix} $$

$$ {}^{M}R_{CR} = \begin{bmatrix} 0.031 & 0.0482 & -0.876 \\ -0.999 & 0.010 & -0.033 \\ 0.012 & 0.876 & 0.482 \end{bmatrix} $$

Pixel scale factors of microscopic camera L and R are

k_{xL}= 0.310 (μm/pixel), k_{yL} = 0.313(μm/pixel);

k_{xR}= 0.310 (μm/pixel), k_{yR} = 0.311 (μm/pixel);

Typical deviation between hole center and sphere center on the image (Δu, Δv) is be (19, -761) for camera L, and (-27, -796) for camera R.

The center point of the sphere is achieved by circle fitting of the selected edge points using the least-square method. Error for the center point of the sphere is very small if number of the selected edge points is increased. So the main error is from the selection of the center point of the hole. Errors between the manual selected center point of the hole is less than 4 pixels on the image.

When, $du_L = dv_L = du_R = dv_R = 4$ (pixel), normalized AO'_1 is calculated to be [-0.0122, -0.0312, -0.9994]^T according to Eq. (9) and normalized AO_1 is calculated to be [-0.0067, -0.0366, -0.9993]^T according to Eq. (3). Deviation angle of AO'_1 from AO_1 is 0.4449°.

When microscopic camera L and microscopic camera R are both moved 300 mm to focus on two different parts of the glass tube. That is, A_1A_{2L} = 300 mm, A_1A_{2R} = 300 mm. Typical deviation between upper point on the glass tube and lower point on the glass tube on the image (Δu, Δv) is (16, -623) for camera L, and (-12, -660) for camera R.

For the manual selection of points on the glass tube, errors are less than 4 pixels on the image.

When, $du_L = du_R = dv_L = dv_R = 4$ (pixel), normalized BA'_1, is calculated to be [-0.0118, -0.0174, -0.9998] ^{T} according to Eq. (9) and normalized BA_1 is calculated to be [-0.0064, -0.0228, -0.9997]^T according to Eq. (5). Deviation angle of BA'_1 from BA_1 is 0.4354°.

5. Pose Aligning

Pose aligning of the glass tube and the hole on the sphere is carried out by adjusting pose of the hole, AO_1, to align it to pose of the glass tube, BA_1.

To align vector AO_1 to vector BA_1, the rotary axis and rotary angle can be calculated by the following equation.

$$ \begin{cases} f = AO_1 \times BA_1 \\ \theta = \arccos\left(\dfrac{AO_1 \cdot BA_1}{\|AO_1\| \|BA_1\|} \right) \end{cases} \tag{10} $$

where, f is the rotary axis, and θ is the angle between vector AO_1 and vector BA_1, and it is also the rotary angle.

Since the angle θ between vector AO_1 and vector BA_1 is small, so $\sin\theta \approx \theta$, $\cos\theta \approx 1$. The rotary matrix for the rotation around axis f for the angle θ is

$$ Rot(f,\theta) \approx \begin{bmatrix} 1 & -f_z\theta & f_y\theta \\ f_z\theta & 1 & -f_x\theta \\ -f_y\theta & f_x\theta & 1 \end{bmatrix} \tag{11} $$

where, $Rot(f, \theta)$ is the rotary matrix for the rotation around axis f for the angle θ, and f_x, f_y, f_z are elements of the normalized rotary axis vector f.

In the microassembly task, the sphere is placed on the sphere gripper carefully with the hole on it facing upwards, and the glass tube is mounted vertically downwards. So vector AO_1 and vector BA_1 are almost parallel to z axis of the manipulator coordinates, which also means that the rotary axis vector f is almost vertical to z axis. So the third element f_z of f is almost equal to 0. The adjusting angles of the platform can be determined as follows.

$$ \begin{cases} \theta_x = f_x\theta \\ \theta_y = f_y\theta \end{cases} \tag{12} $$

where, θ_x is the rotary angle of the pose adjusting platform around x axis, and θ_y is the rotary angle of the pose adjusting platform around y axis.

6. Experiments

6.1 Experiment system

An experiment system (as shown in Fig. 4) was established according to the scheme given in section 2. In the experiment system, there were two 120× magnification microscopic cameras (Navitar 12X combined with Mitutoyo M84010711) and a stereo microscope (Zeiss 2000-C). The stereo microscope was used for the initiation of the pose measurement task, which was, to bring the glass tube to the vicinity of the hole on the sphere. The 3-DOF glass tube manipulator was Sutter MP-285, and it had a travel of 2.54 cm with a resolution of 0.04 mm. The pose adjusting platform had two rotary degrees of freedom, one was around the x axis of the manipulator, the other was around the y axis of the manipulator.

6.2 Repetitive pose measuring experiments and verification experiments

10 consecutive experiments of measuring the pose of the hole on the sphere were conducted, and normalized pose vector of the hole, AO_1, in the manipulator coordinates calculated by Eqs. (1)~(3) are listed in Table 1.

Mean value of the normalized pose vectors of the hole was [0.0050,

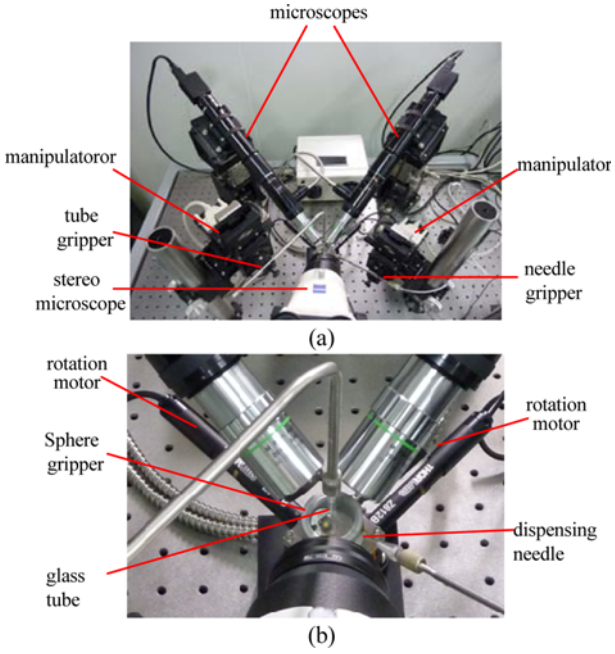

Fig. 4 Experiment system; (a) Whole microassembly platform, (b) Enlarged microassembly area

Table 1 Repetitive pose measuring results of the hole on the sphere

Index	Normalized hole pose vector AO_1
1	$[0.0066, -0.0589, 0.9982]^T$
2	$[0.0064, -0.0552, 0.9985]^T$
3	$[0.0067, -0.0585, 0.9983]^T$
4	$[0.0068, -0.0563, 0.9984]^T$
5	$[0.0042, -0.0550, 0.9985]^T$
6	$[0.0097, -0.0553, 0.9984]^T$
7	$[0.0036, -0.0635, 0.9980]^T$
8	$[0.0012, -0.0603, 0.9982]^T$
9	$[0.0036, -0.0618, 0.9981]^T$
10	$[0.0010, -0.0574, 0.9984]^T$

$-0.0582, 0.9983]^T$.

Angle errors of the normalized pose vectors of the hole from mean value were:

(0.2418, 0.2927, 0.2403, 0.2661, 0.2899, 0.3868, 0.3828, 0.3300, 0.3117, 0.3203)°

Mean angle error was 0.3062°, maximum angle error was 0.3868°, and the variance of the angle errors was 0.0026. The repetitive pose measuring results of the hole indicated that our method had good repetitive accuracy, and the experimental measuring results were in consistency with analytical results.

Fig. 5 is the graphical expression of repetitive pose measuring results of the hole on the sphere.

10 consecutive experiments of measuring the pose of the glass tube were conducted. The pose vector BA_1 of the glass tube in the manipulator coordinates calculated by Eqs. (1), (4), (5) are listed in Table 2.

Mean value of the normalized pose vectors of the glass tube was $[0.0061, -0.0155, 0.9999]^T$

Angle errors of the normalized pose vectors of the glass tube from mean value were:

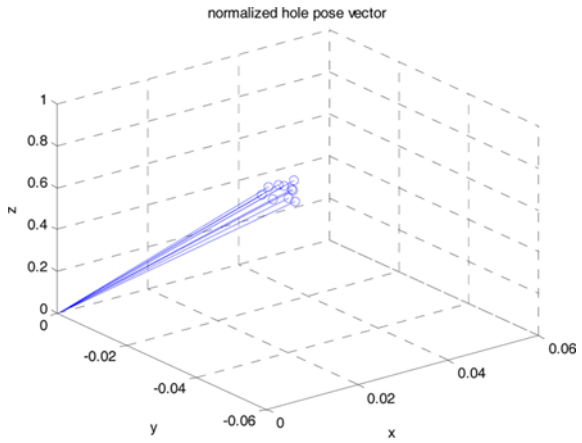

Fig. 5 Repeated pose measuring results of the hole on the sphere

Table 2 Repetitive pose measuring results of the glass tube

Index	Normalized tube pose vector BA_1
1	$[0.0034, -0.0160, 0.9999]^T$
2	$[0.0061, -0.0121, 0.9999]^T$
3	$[0.0026, -0.0152, 0.9999]^T$
4	$[0.0069, -0.0151, 0.9999]^T$
5	$[0.0056, -0.0121, 0.9999]^T$
6	$[0.0095, -0.0174, 0.9998]^T$
7	$[0.0073, -0.0151, 0.9999]^T$
8	$[0.0048, -0.0152, 0.9999]^T$
9	$[0.0062, -0.0172, 0.9998]^T$
10	$[0.0083, -0.0198, 0.9998]^T$

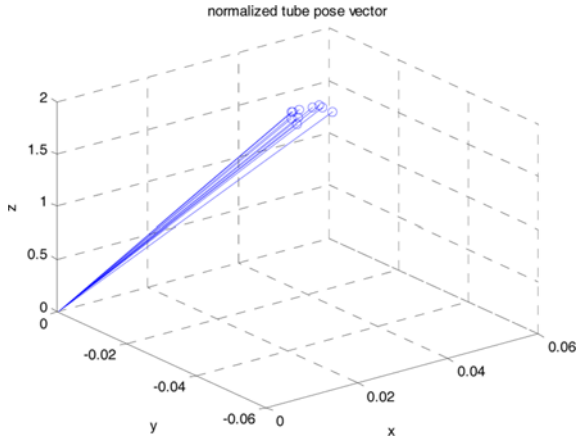

Fig. 6 Repetitive pose measuring results of the glass tube

(0.2289, 0.2616, 0.2630, 0.1776, 0.2597, 0.2818, 0.1857, 0.1859, 0.1946, 0.3240)°

Mean angle error was 0.2363°, maximum angle error was 0.3240°, and the variance of the angle errors was 0.0024. The repetitive glass tube pose measuring results indicated that our method had good repetitive accuracy, and the experimental measuring results were in consistency with analytical results.

Fig. 6 was the graphical expression of repetitive pose measuring results of the glass tube.

Two sets of verification experiments were conducted. One was to

Table 3 Results of verification experiments of rotation around x axis

Measured hole pose vector	Real hole pose vector
[0.0125, -0.1673, 0.9858] ^{T}	[0.0127, -0.1719, 0.9850] ^{T}
[0.0108, -0.1569, 0.9876] ^{T}	[0.0127, -0.1547, 0.9879] ^{T}
[0.0109, -0.1376, 0.9904] ^{T}	[0.0127, -0.1375, 0.9904] ^{T}
[0.0025, -0.1260, 0.9920] ^{T}	[0.0127, -0.1202, 0.9927] ^{T}
[0.0096, -0.1088, 0.9940] ^{T}	[0.0127, -0.1028, 0.9946] ^{T}
[0.0059, -0.0878, 0.9961] ^{T}	[0.0127, -0.0854, 0.9963] ^{T}
[0.0089, -0.0746, 0.9972] ^{T}	[0.0127, -0.0680, 0.9976] ^{T}
[0.0032, -0.0530, 0.9986] ^{T}	[0.0127, -0.0506, 0.9986] ^{T}
[0.0081, -0.0377, 0.9993] ^{T}	[0.0127, -0.0332, 0.9994] ^{T}

Table 4 Results of verification experiments of rotation around y axis

Measured hole pose vector	Real hole pose vector
[0.0127, -0.1891, 0.9819]^T	[0.0127, -0.1891, 0.9819]^T
[-0.0012, -0.1854, 0.9827]^T	[-0.0044, -0.1891, 0.9819]^T
[-0.0141, -0.1797, 0.9836]^T	[-0.0216, -0.1891, 0.9817]^T
[-0.0340, -0.1869, 0.9818]^T	[-0.0387, -0.1891, 0.9812]^T
[-0.0547, -0.1820, 0.9818]^T	[-0.0558, -0.1891, 0.9804]^T
[-0.0654, -0.1881, 0.9800]^T	[-0.0729, -0.1891, 0.9792]^T
[-0.0824, -0.1910, 0.9781]^T	[-0.0900, -0.1891, 0.9778]^T
[-0.0964, -0.1909, 0.9769]^T	[-0.1071, -0.1891, 0.9761]^T
[-0.1163, -0.1948, 0.9739]^T	[-0.1241, -0.1891, 0.9741]^T
[-0.1376, -0.1982, 0.9705]^T	[-0.1411, -0.1891, 0.9718]^T

rotate the pose adjusting platform around x axis, and compare the measured results and the theoretical results of the hole pose. The other set was to rotate the pose adjusting platform around y axis, and compare the measured poses and the real poses of the hole.

Real pose of the hole was determined in the following way. At the beginning, pose of the hole was measured 10 times and the mean value was chosen to be the initial pose of the hole. Then after rotation around x or y axis, the hole pose could be calculated with the rotation angle. Since the pose adjusting platform has good rotation accuracy, the hole pose calculated with the rotation angle was considered the real pose of the hole after rotation.

9 different rotation angles around x axis were tested, and the results are listed in Table 3. All the measured pose vectors of the hole and the real pose vectors of the hole were normalized.

Angles between the measured pose vectors of the hole and the real pose vectors were:

(0.2699, 0.1645, 0.1046, 0.6741, 0.3898, 0.4132, 0.4332, 0.5618, 0.3693)^o

Mean angle error was 0.3756^o. The variance of the angle errors was 0.0322.

9 different rotation angles around y axis were tested, and the results are listed in Table 4.

Angles between the measured pose vectors of the hole and the real pose vectors were:

(0.2834, 0.6994, 0.3015, 0.4190, 0.4396, 0.4499, 0.6216, 0.5519, 0.5613)^o

Mean angle error was 0.4809^o. The variance of the angle errors was 0.0196.

Figs. 7 and 8 are graphical expressions of the comparisons for the two sets of verification experiments.

The two sets of verification experiments results show that our pose measuring method for the hole on the sphere has less than 0.7^o error. In our microassembly task of inserting the glass tube into the sphere with direction of the glass tube towards the center of the sphere, the relative poses of the two objects in the universal coordinates are important. In our pose measuring method, pose of the hole on the sphere and pose of the glass tube were all calculated and expressed in the manipulator coordinates. The error of the angle between the two measured poses is ensured to be less than 0.7^o.

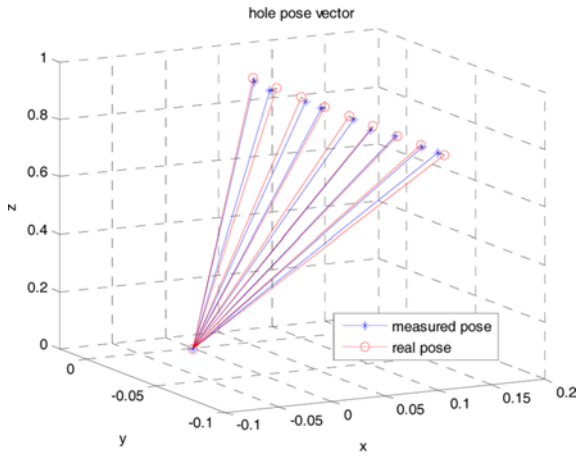

Fig. 7 Comparison results between measured values and real values for rotation around x axis experiments

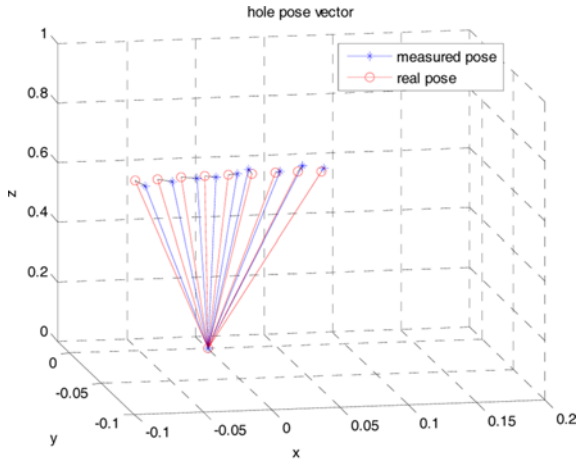

Fig. 8 Comparison results between measured values and real values for rotation around y axis experiments

6.3 Pose aligning experiments

Pose aligning experiments were conducted using our pose measuring and aligning methods. Figs. 9~12 are pose measuring process for the hole on the sphere and the glass tube before pose aligning. Figs. 13 and 14 are pose measuring process for the hole on the sphere after pose aligning. From Figs. 9 to 14, (a) and (b) are the corresponding images from microscopic camera L and microscopic camera R, respectively.

To get the center of the sphere O_1, circle fitting was first conducted when the microscopic camera L (left image) and microscopic camera R (right image) were focused on the outer diameter of the sphere

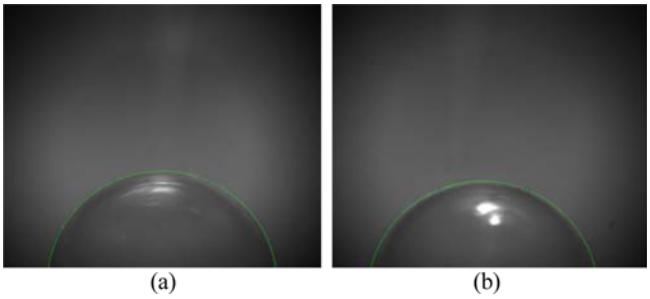

Fig. 9 Points on the outer edge of the sphere were selected

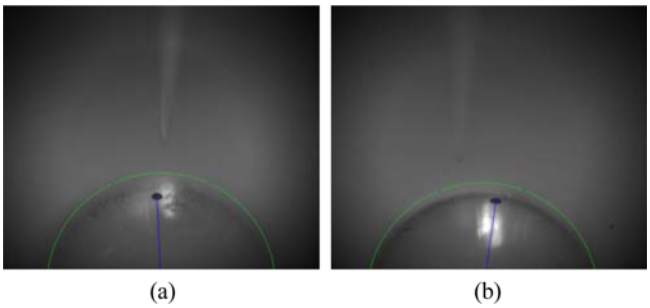

Fig. 10 The hole center point was selected

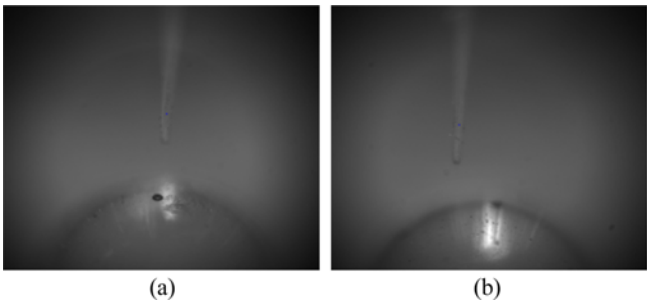

Fig. 11 First point on the glass tube was selected

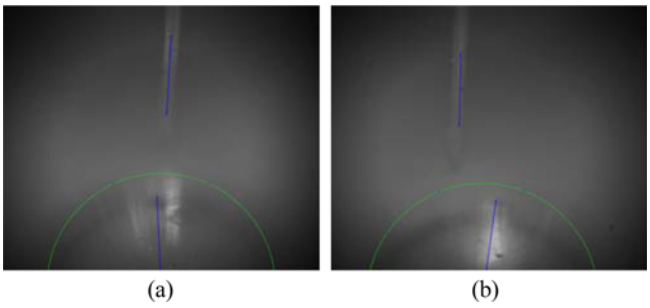

Fig. 12 Second point on the glass tube was selected

respectively. The edge points needed to fit the outline of the sphere was selected manually, after the edge of the sphere was focused, as shown in Fig. 9.

Microscopic cameras were moved to focus on the hole respectively, and the hole center on the image was select. After the center of the hole

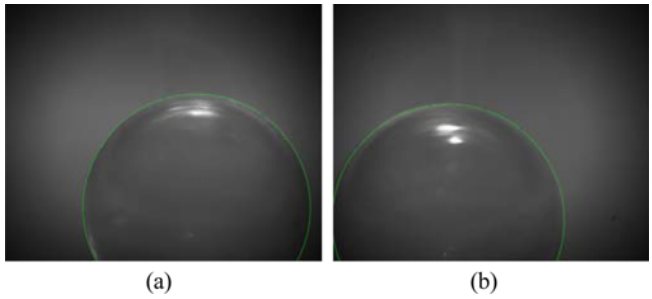

Fig. 13 Points on the outer edge of the sphere were selected

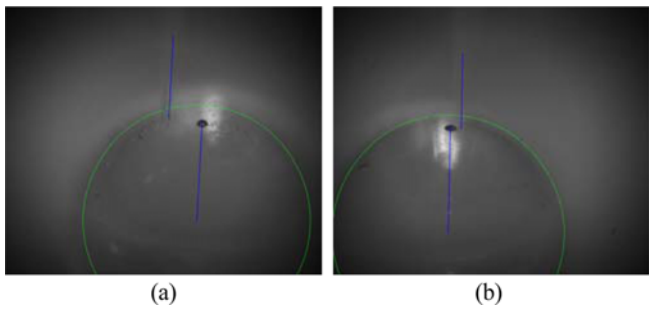

Fig. 14 The hole center point was selected

was selected, the pose of the hole on the sphere could be calculated, as shown in Fig. 10.

The microscopic cameras were moved to focus on the lower part of the glass tube respectively, and the center point of the focused part of the glass tube was selected, as shown in Fig. 11.

Then, the microscopic cameras were moved backward for 300 mm along its optical axis to focus on the upper part of the glass tube, and the center point of the focused part of the glass tube was selected. After two points were selected on the glass tube, the pose of the glass tube could be calculated, as shown in Fig. 12.

Pose measuring results for the hole on the sphere and the glass tube are as follows.

Pose vector of the hole on the sphere AO_1 = [-3095.1, 5540.5, 51267.0]^T (mm).

Normalized AO_1: [-0.0599, 0.1073, 0.9924]^T.

Pose vector of the glass tube BA_1 = [988.6, 374.7, 32650.8]^T (mm).

Normalized BA_1: [0.0303, 0.0115, 0.9995]^T.

Angle between the pose vector of the hole on the sphere and the pose vector of the glass tube was 7.55°.

Normalized rotary axis vector f = [0.7288, 0.6840, -0.0300]^T.

The aligning actions were calculated to be θ_x=5.50°, θ_y=5.16°.

After the actions of pose adjusting platform, the pose of the hole was measured again. Pose measuring results for the hole on the sphere after aligning are as follows.

Pose vector of the hole on the sphere AO_1 = [1776.4, 727.4, 56929.8]^T (mm).

Normalized AO_1: [0.0312, 0.0128, 0.9994]^T.

Since the tube pose had not changed, its pose vector remained the same. Angle between the pose vector of the hole on the sphere and the pose vector of the glass tube was 0.09°.

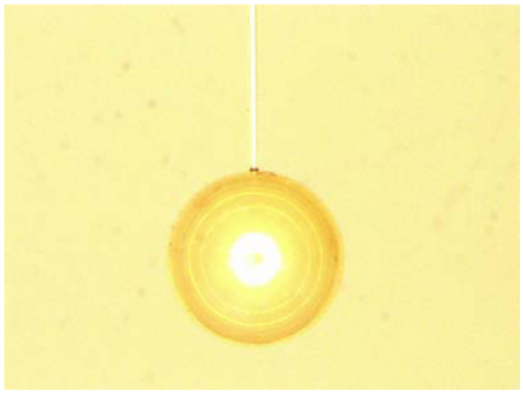

Fig. 15 Pose aligned assembly using our method

It is notice that vectors AO_{2L} and BA_{2L}, AO_{2R} and BA_{2R} on the image were aligned from comparison of Figs. 12 and 14.

The assembled sphere and glass tube can also demonstrate that our pose measuring and aligning method is very effective in improving the assembly quality of the two components. Fig. 15 is the assembled components whose assembly quality was ensured by our pose measuring and aligning method. Clearly, our proposed pose measuring and aligning has achieved good pose aligning accuracy.

7. Conclusions

Since the microscope has a small depth of field, clear image of the whole micro components can not be achieved, and only part of the micro components can be viewed clearly. This makes the pose measuring in microassembly a difficult task. A novel 3-D pose measuring method is proposed in this paper, in which two microscopic cameras are used to get the projection vectors of the pose vector of the glass tube and the pose vector of the hole on the sphere. Pose vector of the measured object is determined by the intersection of the two planes, each one containing the projection vector of the pose vector and the optical axis of the microscopic camera. Error analysis for the pose measuring method is conducted and repeated measuring experiments and verification experiments are carried out. Analytical results and experiments results are in accordance. Both analysis and experiments indicate that our pose measuring method can achieve less than 0.7^{o} error.

ACKNOWLEDGEMENT

This work is supported by the National Natural Science Foundation of China under Grant 61227804 and 61105036, and the China Postdoctoral Science Foundation.

REFERENCES

1. Das, A. N., Zhang, P., Lee, W. H., Popa, D., and Stephanou, H., "μ^3: Multiscale, Deterministic Micro-Nano Assembly System for Construction of On-Wafer Microrobots," Proc. of IEEE International Conference on Robotics and Automation, pp. 461-466, 2007.
2. Wang, L., Mills, J. K., and Cleghorn, W. L., "Automatic Microassembly Using Visual Servo Control," IEEE Transactions on Electronics Packaging Manufacturing, Vol. 31, No. 4, pp. 316-325, 2008.
3. Wang, L., Ren, L., Mills, J. K., and Cleghorn, W. L., "Automated 3-D Micrograsping Tasks Performed by Vision-based Control," IEEE Transactions on Automation Science and Engineering, , Vol. 7, No. 3, pp. 417-426, 2010.
4. Tamadazte, B., Dembélé, S., Fortier, G., and Fort-Piat, L., "Automatic Micromanipulation Using Multiscale Visual Servoing," Proc.of IEEE International Conference on Automation Science and Engineering, pp. 977-982, 2008.
5. Zeng, X., Huang, X., and Wang, M., "Micro-Assembly of Micro Parts using Uncalibrated Microscopes Visual Servoing Method," Information Technology Journal, Vol. 7, No. 3, pp. 497-503, 2008.
6. Borchert, G., Burisch, A., and Raatz, A., "Apis-A Miniaturized Robot for Precision Assembly with Low-Cost Piezoelectric Motors," Int. J. Precis. Eng. Manuf., Vol. 12, No. 4, pp. 629-634, 2011.
7. Kim, M. G., Hong, Y. S., and Lim, E. J., "Position and Orientation Detection of Capsule Endoscopes in Spiral Motion," Int. J. Precis. Eng. Manuf., Vol. 11, No. 1, pp. 31-37, 2010.
8. Yun-feng, Z., Gan-lin, S., and Bing, J., "A Dynamic-Template-Library based Method to Measure the Pose of Maneuvering Target," Proc. of 4th IEEE Conference on Industrial Electronics and Applications, pp. 2080-2084, 2009.
9. Xu, W., Xue, Q., Liu, H., Du, X., and Liang, B., "A Pose Measurement Method of a Non-Cooperative Geo Spacecraft based on Stereo Vision," Proc. of 12th International Conference on Control Automation Robotics & Vision, pp. 966-971, 2012.
10. Assa, A. and Janabi-Sharifi, F., "A Robust Vision-based Sensor Fusion Approach for Real-Time Pose Estimation," IEEE Transactions on Cybernetics, Vol. 44, No. 2, pp. 217-227, 2014.
11. Kyriakoulis, N. and Gasteratos, A., "Color-based Monocular Visuoinertial 3-D Pose Estimation of a Volant Robot," IEEE Transactions on Instrumentation and Measurement, Vol. 59, No. 10, pp. 2706-2715, 2010.
12. Katsuki, R., Ota, J., Mizuta, T., Kito, T., Arai, T., et al., "Design of an Artificial Mark to Determine 3D Pose by Monocular Vision," Proc. of IEEE International Conference on Robotics and Automation, Vol. 1, pp. 995-1000, 2003.
13. Okafor, A. C. and Ertekin, Y. M., "Vertical Machining Center Accuracy Characterization using Laser Interferometer: Part 2. Angular Errors," Journal of Materials Processing Technology, Vol. 105, No. 3, pp. 407-420, 2000.
14. Zhang, Y. N., Chen, X., Song, W., and Shen, L. Y., "Visual Measurement of Micro-Target Pose in ICF Experiment," Proc. of IEEE International Conference on Computer Science and Automation

Engineering, Vol. 1, pp. 102-106, 2012.

15. Wang, L., Mills, J. K., and Cleghorn, W. L., "Assembly of Three-Dimensional Microsystems Using a Hybrid Manipulation Strategy," Proc. of IEEE International Conference on Mechatronics and Automation, pp. 545-550, 2008.

16. Li, F., Xu, D., Shi, Y., and Zhang, Z., "Motion-based Microscopic Camera Calibration and Application on Micro Tube-Hole Insertion," Optical Engineering, Vol. 53, No. 5, Paper No. 053103, 2014.

APPENDIX

$$
\begin{aligned}
n'_{HL} &= AO'_{2L} \times V'_{zL} \\
&= [\Delta x'_{mL}, \Delta n'_{mL}, \Delta z'_{mL}]^T \times [a_{xL}, a_{yL}, a_{zL}]^T \\
&= [\Delta n'_{mLx}, \Delta n'_{mLy}, \Delta n'_{mLz}]^T \\
&= \begin{bmatrix}
a_{zL}[n_{yL}k_{xL}(\Delta u_L + du_L) + o_{yL}k_{yL}(\Delta v_L + dv_L)] \\
-a_{yL}[n_{zL}k_{xL}(\Delta u_L + du_L) + o_{zL}k_{yL}(\Delta v_L + dv_L)] \\
\\
a_{zL}[n_{xL}k_{xL}(\Delta u_L + du_L) + o_{xL}k_{yL}(\Delta v_L + dv_L)] \\
-a_{xL}[n_{zL}k_{xL}(\Delta u_L + du_L) + o_{zL}k_{yL}(\Delta v_L + dv_L)] \\
\\
a_{yL}[n_{xL}k_{xL}(\Delta u_L + du_L) + o_{xL}k_{yL}(\Delta v_L + dv_L)] \\
-a_{xL}[n_{yL}k_{xL}(\Delta u_L + du_L) + o_{yL}k_{yL}(\Delta v_L + dv_L)]
\end{bmatrix}
\end{aligned} \tag{A1}
$$

$$
\begin{aligned}
n'_{HR} &= AO'_{2R} \times V'_{zR} \\
&= [\Delta x'_{mR}, \Delta n'_{mR}, \Delta z'_{mR}]^T \times [a_{xR}, a_{yR}, a_{zR}]^T \\
&= [\Delta n'_{mRx}, \Delta n'_{mRy}, \Delta n'_{mRz}]^T \\
&= \begin{bmatrix}
a_{zR}[n_{yR}k_{xR}(\Delta u_R + du_R) + o_{yR}k_{yR}(\Delta v_R + dv_R)] \\
-a_{yR}[n_{zR}k_{xR}(\Delta u_R + du_R) + o_{zR}k_{yR}(\Delta v_R + dv_R)] \\
\\
a_{zR}[n_{xR}k_{xR}(\Delta u_R + du_R) + o_{xR}k_{yR}(\Delta v_R + dv_R)] \\
-a_{xR}[n_{zR}k_{xR}(\Delta u_R + du_R) + o_{zR}k_{yR}(\Delta v_R + dv_R)] \\
\\
a_{yR}[n_{xR}k_{xR}(\Delta u_R + du_R) + o_{xR}k_{yR}(\Delta v_R + dv_R)] \\
-a_{xR}[n_{yR}k_{xR}(\Delta u_R + du_R) + o_{yR}k_{yR}(\Delta v_R + dv_R)]
\end{bmatrix}
\end{aligned} \tag{A2}
$$

$$
\begin{aligned}
ao_{1x} = {} & [(a_{zL}n_{xL}k_{xL} - a_{xL}n_{zL}k_{xL})(\Delta u_L + du_L) + (a_{zL}o_{xL}k_{yL} - a_{xL}o_{zL}k_{yL})(\Delta v_L + dv_L)] \\
& [(a_{yR}n_{xR}k_{xR} - a_{xR}n_{yR}k_{xR})(\Delta u_R + du_R) + (a_{yR}o_{xR}k_{yR} - a_{xR}o_{yR}k_{yR})(\Delta v_R + dv_R)] \\
& -[(a_{yL}n_{xL}k_{xL} - a_{xL}n_{yL}k_{xL})(\Delta u_L + du_L) + (a_{yL}o_{xL}k_{yL} - a_{xL}o_{yL}k_{yL})(\Delta v_L + dv_L)] \\
& [(a_{zR}n_{xR}k_{xR} - a_{xR}n_{zR}k_{xR})(\Delta u_R + du_R) + (a_{zR}o_{xR}k_{yR} - a_{xR}o_{zR}k_{yR})(\Delta v_R + dv_R)]
\end{aligned} \tag{A3}
$$

$$
\begin{aligned}
ao_{1y} = {} & [(a_{yL}n_{xL}k_{xL} - a_{xL}n_{yL}k_{xL})(\Delta u_L + du_L) + (a_{yL}o_{xL}k_{yL} - a_{xL}o_{yL}k_{yL})(\Delta v_L + dv_L)] \\
& [(a_{zR}n_{yR}k_{xR} - a_{yR}n_{zR}k_{xR})(\Delta u_R + du_R) + (a_{zR}o_{yR}k_{yR} - a_{yR}o_{zR}k_{yR})(\Delta v_R + dv_R)] \\
& -[(a_{zL}n_{yL}k_{xL} - a_{yL}n_{zL}k_{xL})(\Delta u_L + du_L) + (a_{zL}o_{yL}k_{yL} - a_{yL}o_{zL}k_{yL})(\Delta v_L + dv_L)] \\
& [(a_{yR}n_{xR}k_{xR} - a_{xR}n_{yR}k_{xR})(\Delta u_R + du_R) + (a_{yR}o_{xR}k_{yR} - a_{xR}o_{yR}k_{yR})(\Delta v_R + dv_R)]
\end{aligned} \tag{A4}
$$

$$
\begin{aligned}
ao_{1z} = {} & [(a_{zL}n_{yL}k_{xL} - a_{yL}n_{zL}k_{xL})(\Delta u_L + du_L) + (a_{zL}o_{yL}k_{yL} - a_{yL}o_{zL}k_{yL})(\Delta v_L + dv_L)] \\
& [(a_{zR}n_{xR}k_{xR} - a_{xR}n_{zR}k_{xR})(\Delta u_R + du_R) + (a_{zR}o_{xR}k_{yR} - a_{xR}o_{zR}k_{yR})(\Delta v_R + dv_R)] \\
& -[(a_{zL}n_{xL}k_{xL} - a_{xL}n_{zL}k_{xL})(\Delta u_L + du_L) + (a_{zL}o_{xL}k_{yL} - a_{xL}o_{zL}k_{yL})(\Delta v_L + dv_L)] \\
& [(a_{zR}n_{yR}k_{xR} - a_{yR}n_{zR}k_{xR})(\Delta u_R + du_R) + (a_{zR}o_{yR}k_{yR} - a_{yR}o_{zR}k_{yR})(\Delta v_R + dv_R)]
\end{aligned} \tag{A5}
$$